Biophysical elucidation of the mechanism of enhanced drug release and topical delivery from polymeric film-forming systems

Hazel Garvie-Cook[1,2], Kit Frederiksen[2,3], Karsten Petersson[3], Richard H. Guy[2,*], Sergey N. Gordeev[1].

[1]University of Bath, Department of Physics, Bath, BA2 7AY, U.K.

[2]University of Bath, Department of Pharmacy & Pharmacology, Bath, BA2 7AY, U.K.

[3]LEO Pharma A/S, Industriparken 55, DK-2750 Ballerup, Denmark.

*Corresponding author: Richard H. Guy, Department of Pharmacy & Pharmacology, University of Bath, Claverton Down, Bath, BA2 7AY, U.K. Tel.: +44.1225.384901. E-mail address: r.h.guy@bath.ac.uk

Authors' contributions: HG-C performed the atomic force microscopy and Raman spectroscopy; KF undertook the experiments evaluating drug release and skin penetration from the polymeric film-forming systems. These efforts reflect separate but equally important contributions to the paper. Both HG-C and KF participated with KP, RHG and SNG in the analysis and interpretation of the data obtained, and in the preparation of the paper. KP, RHG and SNG were primarily responsible for the study concept and design.

Abstract

The effect of incorporating the lipidic medium-chain triglyceride (MCT) into polymeric film-forming systems (FFS) for topical drug delivery has been evaluated. First, the *in vitro* release of betamethasone-17-valerate (BMV), a representative dermatological drug, was determined from FFS comprising either hydrophobic polyacrylate co-polymers, or hydrophilic hydroxypropyl cellulose, with and without MCT. Release was enhanced from both polymers in the presence of MCT. Atomic force microscopy imaging and nanoindentation of FFS with MCT revealed two-phase structured films with softer inclusions (0.5 to 4 μm in diameter) surrounded by a more rigid structure. Chemical mapping with Raman micro-spectroscopy showed that MCT was primarily confined to the inclusions within the polymer, which predominated in the surrounding film. BMV was distributed throughout the film but was more concentrated outside the inclusions. Furthermore, while BMV dissolved better into the hydrophobic films, it was more soluble in the MCT inclusions in hydrophilic films, suggesting its increased availability for diffusion from these softer regions of the polymer and explaining the release enhancement observed. Second, *ex vivo* skin penetration studies clearly revealed that uptake of BMV was higher from hydrophobic FFS than that from the more hydrophilic polymer due, at least in part, to the superior anti-nucleation efficiency of the former. Drug was quickly taken up into the SC from which it then diffused continuously over a sustained period into the lower, viable skin layers. In the presence of MCT, the overall uptake of BMV was increased and provides the basis for further optimisation of FFS as simple, convenient and sustained formulations for topical therapy.

Keywords: Polymeric film-forming systems; topical drug delivery; atomic force microscopy; Raman chemical mapping; supersaturation; anti-nucleation

Introduction

The stratum corneum (SC) forms the outermost layer of the skin and provides a barrier to the delivery of adequate therapeutic drug concentrations into the skin. Usually, only a small percentage of the amount of drug substance applied on the skin is delivered to the target site, with the rest becoming unavailable for delivery because of surface loss and/or changes in the vehicle that prevent drug from diffusing into and through the skin [1, 2]. The treatment of dermatological diseases would be improved, therefore, if an increase or prolongation of drug delivery into the skin from topically applied formulations were possible. Polymeric film-forming systems (FFS), created *in situ* after administration, offer a more efficient and patient-friendly topical formulation with the potential to increase and/or sustain drug delivery and permit less frequent dosing [3-7]. Additionally, incorporation of plasticisers into FFS has been demonstrated to increase the *in vitro* release of incorporated drugs [8-11]. Given that increased BMV release and skin uptake with increasing plasticiser lipophilicity and higher MCT concentrations had been observed in earlier work [7, 12], this investigation primarily focused on the effect of the lipidic medium-chain triglyceride (MCT), which is a well-known excipient in dermatologic formulations.

Atomic force microscopy (AFM) can provide both topographical and mechanical information on polymeric films at the nanoscale [11]. AFM imaging reveals film homogeneity, a key feature related to the contact between the skin and the drug delivery system. Nanoindentation uses the sensitivity of the AFM cantilever to small forces, and permits local mechanical properties, such as elastic modulus and hardness, to be determined. The approach has previously been applied to pharmaceutical excipients, such as sucrose [13], and to determine the effect of a topical cream on skin mechanics [14]. Chemical maps of polymeric films can be determined by Raman micro-spectroscopy and the spatial distribution of the constituents determined from characteristic spectral features. This information, in combination with data from AFM, provides insight into the mechanism of drug release from polymer films, and the impact of FFS composition (e.g., presence or absence of MCT).

Here, the anticipated enhancement and prolongation of drug release due to the incorporation of the lipidic MCT into polymeric film-forming systems was studied using betamethasone-17-valerate (BMV) as a model compound. In parallel, AFM and Raman micro-spectroscopy were used, respectively, to elucidate mechanistic information about the mechanical properties and the physical distribution of the constituents of the films.

FFS are typically classified as either hydrophilic or hydrophobic depending on the water-solubility of the film-forming polymer and the substantivity of the formed film on the skin (defined as its persistence and resistance to removal, e.g., by washing, perspiration and wear). Hydrophilic films must establish a drug reservoir in the skin, due to their low water-resistance and low substantivity. Hydrophobic films, having greater water-resistance and substantivity, can, in principle, form a drug reservoir externally on the skin surface as well as within the skin itself. In this case, the two reservoirs are not easily distinguished, as the partitioning of drug substance from the external film into the SC and subsequently into the deeper skin layers are interdependent and intimately related. A further potential advantage of FFS is that evaporation of its volatile constituent(s) immediately post-application can lead to supersaturation of the drug. While such a metastable state is thermodynamically unfavourable [15], rapid recrystallization of the drug [16, 17] may be retarded by excipients that inhibit nucleation, such as certain polymers that are known components of previously investigated FFS [15, 17-19]. An obvious design attribute of a FFS formulation, therefore, is to create a residual film in which the drug remains in a molecular (i.e., solubilised) form able to freely diffuse to the interface with the skin, to partition into the SC, and to continue its

'journey' into the deeper skin layers. The validity of these concepts has been examined via experimental measurements of the skin uptake *ex vivo* of BMV following delivery from selected FFS and from a more conventional, semi-solid, vehicle. This straightforward *ex vivo* study serves, therefore, as a penultimate step in formulation development before undertaking more detailed, *in vivo* experiments in man. Ultimately, it is suggested that the knowledge derived from this work will contribute to the rationale design and optimisation of polymeric FFS that can provide sustained and effective topical therapy over extended periods of time.

Materials and Methods

Materials

Betamethasone-17-valerate (BMV, purity 100%) was purchased from Crystal Pharma SAU (Boecillo, Spain); tritiated [1,2(n)-^{3}H]-betamethasone 17-valerate (17.8 MBq/ml) was prepared by RC TRITEC AG (Teufen, Schwitzerland) and purified by LEO Pharma A/S (Ballerup, Denmark). The polymers used were Eudragit® RS PO (Eudragit) (ammonio methacrylate copolymer type B) from Evonik Röhm GmbH (Darmstadt, Germany), Dermacryl® 79 (Dermacryl) (acrylates/octylacrylamide copolymer) from Akzo Nobel Surface Chemistry AB (Stenungsund, Sweden), and Klucel™ LF (Klucel) (hydroxypropyl cellulose) from Azelis (Lyngby, Denmark). Medium-chain triglyceride (Miglyol 812 N, caprylic/capric triglyceride) was purchased from Sasol (Hamburg, Germany), triethyl citrate (TEC) from Merck (Darmstadt, Germany), and methyl-β-cyclodextrin (MbCD) (Kleptose Crysmeb) from Roquette (Lestrem, France). White, soft paraffin and liquid paraffin were from LEO Pharma A/S (Dublin, Ireland), and Soluene®-350 and Hionic-Fluor were purchased from Perkin Elmer (Skovlunde, Denmark). Sodium acetate trihydrate and all other analytical solvents were purchased from VWR – Bie Berntsen A/S (Herlev, Denmark), Merck (Darmstadt, Germany) and Sigma-Aldrich (Broendby, Denmark).

FFS preparation

Film-forming solutions were prepared by dissolving the polymer, with and without 20% w/w MCT, in absolute ethanol (mixed with 5% w/w water for Eudragit) and stirring overnight until a clear solution was obtained. The concentration of MCT is expressed relative to the dry weight of the polymer. Drug-loaded formulations were prepared by dissolving BMV in the FFS with stirring at a concentration of 1.2% (w/w) (corresponding to 1.0% (w/w) betamethasone), which provided an infinite dose for the *in vitro* release tests.

For the *ex vivo* skin penetration experiments, the effects of incorporating either MCT or the plasticiser, TEC (again at 20 % w/w relative to the dry weight of the polymer) were examined. The BMV mixed into the polymers was doped with the tritiated drug (final strength 1 MBq/g). The formulation compositions tested are in Table 1.

Polarised optical microscopy

Crystallisation of BMV from ethanol and from the polymeric FFS was evaluated with polarised optical microscopy (Nikon Eclipse 80i microscope, Nikon Corporation, Tokyo, Japan) equipped with 10x and 40x objectives. To facilitate visualisation of the crystals, the concentration of the drug in ethanol, 5% w/w Klucel, 5% w/w Eudragit and 15% w/w Eudragit FFS was 6.07% w/w (corresponding to 5% w/w betamethasone). A suitable volume of each solution was distributed on a microscope glass slide and allowed to dry at room temperature. The presence or absence of BMV crystals, and their distribution, was noted.

Table 1 Composition of film-forming systems (all containing 1.2 % w/w BMV) tested in the *ex vivo* penetration experiments.

Formulation constituents (% w/w)							
Polymer		Klucel LF			Eudragit RS		Dermacryl 79
	5.0	5.0	5.0	15.0	15.0	15.0	10.0
Plasticiser/Lipid							
TEC		1.0			3.0		
MCT			1.0			3.0	
Solvent							
EtOH	95.0	94.0	94.0	80.0	77.0	77.0	90.0
Water				5.0	5.0	5.0	

TEC = triethyl citrate; MCT = medium-chain triglyceride; EtOH = absolute ethanol.

Preparation of semi-solid vehicle

White soft paraffin (99.0 % w/w) and liquid paraffin (1.0 % w/w) were mixed at 80°C and allowed to cool completely before further processing. 1.2 % w/w BMV and 1 MBq g^{-1} ^{3}H-BMV were dissolved in ethanol and the solvent was then evaporated in an ultrasound water bath to produce relatively small (<25 µm) BMV crystals. Finally, the solid drug was dispersed in the paraffin ointment using a mortar.

BMV *in vitro* release

The *in vitro* release studies were conducted as previously described [7]. Briefly, experiments were conducted using modified diffusion cells (LEO Pharma A/S, Denmark), with a silicone membrane (Dow Corning® 7-4107 Silicone Elastomer Membrane, 75 µm) separating the applied FFS and the receptor medium (10% w/w solution of methyl-beta-cyclodextrin in acetate buffer pH 4.5).

Atomic Force Microscopy

AFM experiments were carried out using a Multimode Scanning Probe Microscope (Veeco, Plainview, NY) with a Nanoscope IIIA controller and Nanoscope software (Version 7.341).

For AFM imaging and nanoindentation, film forming solutions with and without MCT were spread uniformly onto glass slides heated to 30°C to mimic the temperature of the skin surface. The films were then maintained at this temperature overnight. The final thickness of the prepared films was ~10 µm.

Imaging

Imaging was performed in tapping mode under ambient conditions. 'All in One' AFM probes (AIOAl, Budget Sensors, Sofia, Bulgaria), with nominal spring constants between 0.2 and 40 N/m and resonance frequencies between 15 and 350 kHz, were used for imaging. Images were analysed using Nanoscope Analysis (Version 1.3, Bruker, Billerica, MA).

Nanoindentation

The spring constant of each AFM probe used in this study was determined using a well-accepted approach [20]. Nanoindentation was undertaken (as described elsewhere [11]) with probes having spring constants between 6.1 and 8.5 N/m. The AFM probe tips were modified for these experiments by the electron beam induced deposition (EBID) of amorphous carbon in the chamber of a scanning electron microscope (SEM) (6301F, JEOL, Tokyo, Japan) [21]. The approach makes the probe tips rounded and their radii of curvature can be determined in the SEM. The shape of the indenter could therefore be modelled as spherical. The maximum depth of the subsequent indentation of the polymer films was less than the radii of curvature of the probes selected, ranging from 27 to 80 nm.

During the indentation process, the deflection of the cantilever, the vertical position of the cantilever, and time were recorded. From the resulting deformation-time data, the elastic modulus of the sample was determined using an adaption of the analysis developed by Oyen & Cook [20, 22].

Raman Microscopy

Samples for Raman mapping were prepared as described above but at room temperature. BMV was examined in solution (0.4% w/w in ethanol) and in the solid state (crystalline, as provided by the supplier, and amorphous forms). An amorphous film of BMV was formed by depositing a drop of an ethanolic solution onto a cleaned glass slide [23, 24].

Spectroscopic measurements were performed using a Raman microscope (inVia, Renishaw, Gloucestershire, UK). The excitation source was a laser operating at 532 nm. Initially, Raman spectra of Eudragit, Klucel, MCT, and BMV in the solid state and in solution were obtained using 10% of the maximum laser power available. Characteristic peaks observed in the Raman spectra of MCT and BMV, which were distinct from those seen in the spectra of the polymers, allowed their spatial distribution to be mapped.

Raman maps (30 x 40 μm^2) of polymeric films incorporating MCT were acquired. To increase the resolution, so that the Raman data could complement the AFM images, the excitation laser beam was directed to the sample via a pinhole. This reduced the area from which spectra were obtained to approximately 1 x 1 μm^2 (equal, therefore, to the area of each pixel in the resulting chemical maps). Mapping was performed using the maximum laser power available (~80 mW); no damage to any sample was observed.

The Raman spectra were analysed with Wire 3.4 software (Renishaw). Spectral parameters were defined and fitted to specific scattering peaks for MCT and BMV. The chemical composition of the film could then be mapped by the intensities of the MCT and BMV peaks at each position. The frequency of the BMV peak permitted the physical state of the drug within the films to be inferred.

Skin uptake of BMV *ex vivo*

As the goal was to measure drug delivery into the skin, experiments were performed on isolated, intact porcine ears; pig skin is an accepted surrogate for the human counterpart [1, 25]. Franz diffusion cells with excised skin are commonly used to determine the amount of drug in the SC and the amount that has diffused through the skin into the receptor solution. In the present study, however, as the focus lay in the distribution of BMV in the SC, as opposed to its ability to diffuse through the skin, intact porcine ears were used to simulate the in vivo situation as closely as possible [26, 27]. Radiolabeled BMV allowed facile quantification of drug in the different skin compartments [28]. Initially, drug uptake over 24

hours was assessed but the obvious degeneration of the tissue meant that all subsequent experiments were limited to a shorter duration of 8 hours.

Preparation of pig ears

Porcine ears were obtained from the Danish Meat Trade College (Roskilde, Denmark) shortly after the animals were killed. The ears had been removed before exposure to any high-temperature cleaning procedure so as to preserve the integrity of the skin barrier. The ears were stored at -20°C and thawed slowly at 5°C before cleaning with water and gently trimming away the hair with clippers (Oster, Tennessee, USA). To minimise drying out of the ear during the experiment, the severed surface was wrapped in an isotonic salt-soaked cloth and then sealed with cling film and 3M Transpore™ Medical Tape (Copenhagen, Denmark). The ear was allowed to equilibrate at room temperature for 1-2 hours before application of formulation. To permit sequential measurements at different application times, five sites were delineated on each ear and considerable care was taken to ensure that the films were deposited within the prescribed areas.

Skin penetration experiments

Either 10 µl/cm^2 of FFS was applied evenly on the skin (3.8 cm^2) using a piston pipette (Gilson MICROMANTM pipette, Gilson Inc.), or 10 mg/cm^2 of ointment was spread carefully using a spatula. The Eudragit and Klucel films created *in situ* remained intact while on the surface of the skin. At 15 min, 1 h, 3 h, 6 h and 8 h (Klucel FFS only to 6h) post-application, the remaining formulation was removed. The cleaning procedure ensured that residual formulation from the skin surface, and from skin furrows, was not included when quantifying the amount of drug in the SC [29]. For Klucel films, the skin was wiped with water-soaked cotton pads; for the Eudragit and Dermacryl films, one D-Squame® tape disc, applied with pressure for 10 s (D-Squame® pressure application, Cuderm Corporation), was used to remove the polymers. Ointment was removed by wiping the skin with dry cotton pads.

The SC at the treated skin sites was removed by sequential tape stripping using D-Squame® tape discs, applying a pressure of 225 g/cm^2 for 10 s. The SC sampling site was delimited by a template, which exposed an area smaller than that treated with the formulation. Transepidermal water loss (TEWL) was measured using a VapoMeter (Delfin Technologies, Kuopio, Finland) prior to and at regular intervals during tape stripping which was stopped when the value had increased by 10 times the initial reading or was no longer increasing. This procedure was validated in preliminary experiments following application of placebo Klucel and Eudragit FFS. In these experiments (n = 3 for each FFS), at the conclusion of tape-stripping, skin biopsies were taken and fixed in formalin followed by haematoxylin-eosin staining before microscopic evaluation to confirm the complete removal of SC [28]. The first tape was discarded[1], and BMV was quantified on all subsequent strips. The total number of tapes used depended upon treatment time and individual SC thickness but was never more than 30. On occasion, even though TEWL had not increased to 10x baseline, it was observed that the epidermis began to loosen; in these cases, tape-stripping was terminated

[1] With respect to removal of residual formulation from the skin surface, there remains an open question about whether, subsequent to the cleaning procedure adopted, one or more tape-strips to complete the surface 'decontamination' process should be used. It was decided to take and discard a single tape-strip for this purpose; however, BMV was routinely quantified on this strip to gauge the impact of excluding this amount of drug from the total uptake eventually measured. As expected, this first strip did contain a significant and quite consistent quantity of BMV for the formulations tested; in terms of the total SC uptake, in fact, the first strip contained, on average, 56%, 61%, 29% and 31% for the Klucel, ointment, Eudragit and Dermacryl formulations, respectively. While inclusion of these BMV amounts in the calculated total uptake would have obviously increased somewhat the measured drug 'availability' to the skin, the *relative* performance of the different vehicles examined would not have been affected.

and BMV recovered on that strip was considered to be in the epidermis. Epidermis and dermis were then excised and separated by heat (incubation for 7 min at 60°C and high humidity). For time points up to 8 hours (when the experiment was stopped), the extracted areas of skin were sealed with Parafilm® to prevent the ear from drying out.

Sample analysis

BMV was extracted from SC on the tapes and from the epidermis/dermis using Soluene® 350 (24 h incubation at 50°C). 10 ml of Hionic-Fluor were added to the Soluene extractions and to the cotton pad extracts before analysis by liquid scintillation counting (Tri-Carb 2900 TR Liquid Scintillation Counter, Packard Instrument Company, Meriden, USA). Hionic-Fluor alone provided the necessary background measurements.

Data analysis

All statistical analyses were performed with GraphPad Prism 5.01. Two-way ANOVA ($p < 0.05$) followed by Bonferroni post-test was used to compare means.

Results

BMV release *in vitro*

BMV release was determined for FFS with and without MCT. Previous experiments have investigated BMV release from Eudragit (hydrophobic) and Klucel (hydrophilic) films incorporating the plasticizer TEC [7]. The prepared films all sustained BMV release over 72 hours, with the incorporation of MCT causing significant enhancement that became apparent from about 6 hours into the experiment (Figure 1). Release from Eudragit films followed $t^{½}$ kinetics, consistent with previous observations [7], with MCT resulting in an increase in the rate from 0.45 to 2.19 µg cm^{-2} $h^{-½}$. For the Klucel films, the release was zero-order (again, as had been seen before [7]) and the incorporation of MCT enhanced the rate from 0.58 to 1.56 µg cm^{-2} h^{-1}.

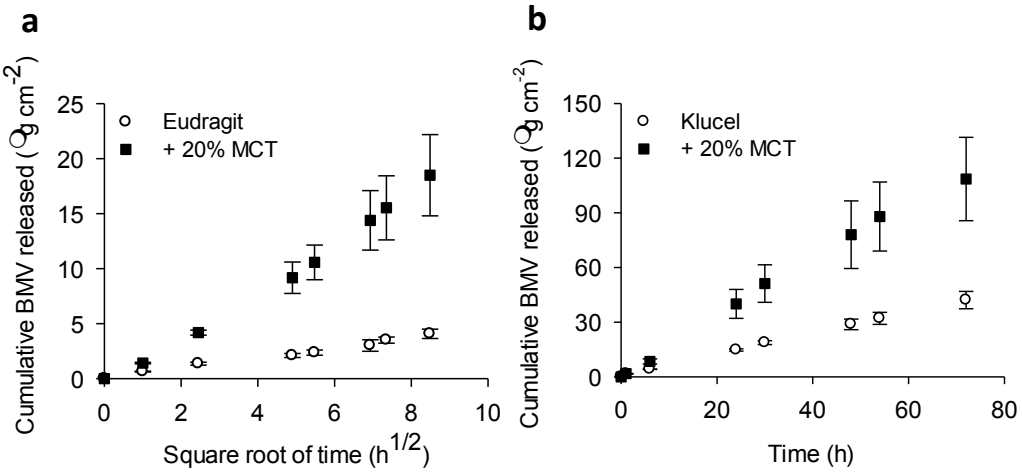

Figure 1. *In vitro* release of BMV from (a) Eudragit, and (b) Klucel film-forming systems with and without medium-chain triglyceride (MCT) (mean ± standard deviation, n=3).

AFM images of polymeric films

The topography of the films deposited on glass slides was imaged with AFM in tapping mode (Figure 2). The Eudragit film without MCT was relatively smooth (variations in height of the observed structural features being only about 1-2 nm) with a root mean square (RMS) roughness of 0.7 nm. Klucel films had a distinctly different, and less smooth appearance, with an RMS roughness of 4.6 nm [11].

Incorporation of MCT (Figure 2) significantly changed the topography of the polymeric films. For Eudragit, there were regions (hereinafter referred to as inclusions) where the structure appeared to dip into the sample surface. These ellipsoidal inclusions ranged from 0.5 to 1.0 μm in diameter. Similar structures were seen in the Klucel films although, in this case, the inclusions appeared above the surrounding material and were larger (2 - 4 μm in diameter) than those observed with Eudragit.

Nanoindentation

During AFM nanoindentation, indents were separated by at least 250 nm along the sample surface to ensure that each new indent would deform a previously unaffected area of the film. The load (*P*) applied to the sample by the probe tip was calculated using the cantilever spring constant. The sample deformation (*h*) at a given cantilever deflection (*D*) was found from the difference in cantilever vertical position between the calibration and sample indentation curves.

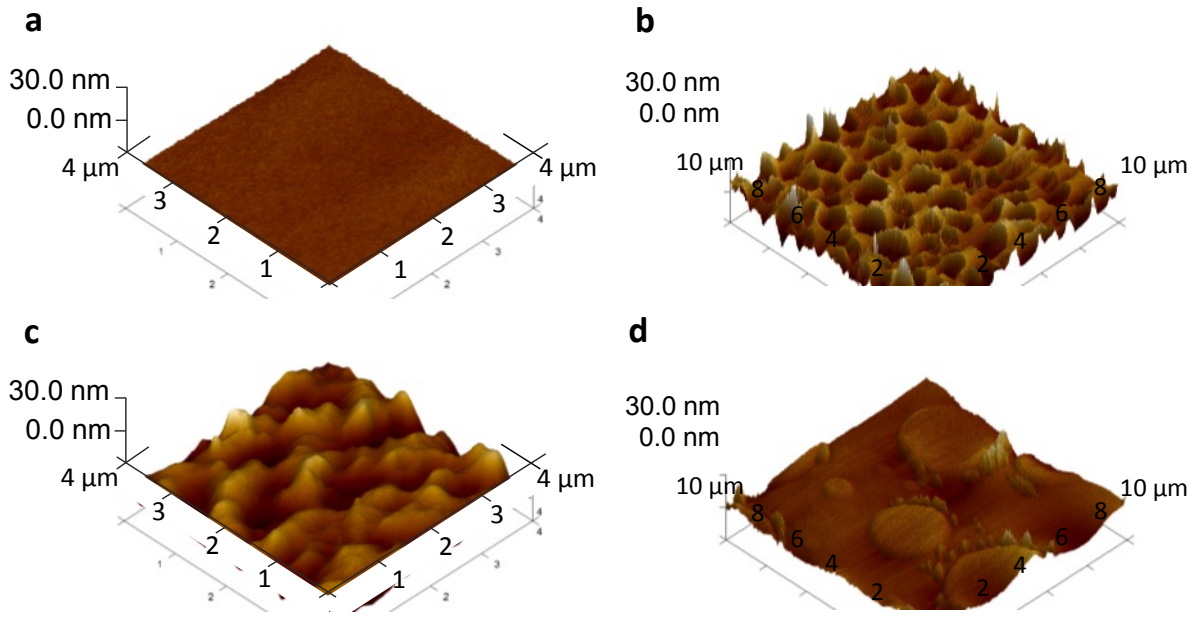

Figure 2. Pseudo 3D AFM images of Eudragit ((a) and (b)) and Klucel ((c) and (d)) FFS, cast onto glass microscope slides, with ((b) and (d)) and without ((a) and (c)) 20% w/w MCT incorporated [7]. The scan size was 4 x 4 μm^2 for the films without MCT and 10 x 10 μm^2 for those with.

The load-deformation behaviour for films with and without MCT (Figure 3) provides the information necessary to select a model with which to fit the data and to extract the elastic moduli of the samples. The results reveal (i) the significantly different nanoindentation behaviour of films incorporating MCT, and (ii) that there is greater deformation at a given

load of the softer inclusions than that of the more rigid surrounding areas (the mechanical properties of which are very similar to those of pure polymer films). For example, at a load of 50 nN, the deformation of Eudragit with 0% MCT (Figure 3(a)) is 2 nm. This is the same as the deformation of areas surrounding the inclusions in Eudragit films containing MCT at this load. The deformation of the inclusions within these films is greater, at 7 nm. Similarly, the deformation of the inclusions within Klucel films incorporating MCT (Figure 3(b)) at a load of 50 nN is 10 nm. This is greater than the deformation in the areas surrounding the inclusions and in Klucel films without MCT; namely, 6 and 5 nm, respectively.

The larger hysteresis in the load-deformation plots from the inclusions compared to the behaviour of films without MCT is also consistent with their more pronounced viscous-plastic behaviour (i.e., that they are 'softer'). The latter can be characterised using an effective hardness (H_e):

$$H_e = P_{max}/A$$

where P_{max} is the maximum load on the sample, and A is the effective projected area of the indent when $P = 0$ [30]. The projected area is calculated from

$$A = (2 \times \pi \times R \times h_f) - (\pi \times h_f^2)$$

where R is the radius of curvature of the indenter and h_f is the residual deformation when $P = 0$. The effective hardness for the inclusions in Eudragit and Klucel films were 0.13 (±0.02) and 0.037 (±0.007) GPa, respectively. In contrast, the corresponding H_e values for the areas surrounding the inclusions were 0.23 (±0.04) and 0.070 (±0.010) GPa. The effective hardnesses of the two polymers demonstrates the softer nature and the more pronounced viscous-plastic behaviour of Klucel films which require a lower load to deform non-elastically. The load-deformation behaviour of the inclusions in Eudragit and Klucel films shows distinct deformation characteristics. This implies that the inclusions not only comprise MCT and BMV, but must also contain some quantity of the respective polymer too.

The Oyen & Cook model, to interpret the nanoindentation data of viscous-elastic-plastic materials, has been adapted for spherical indentation [22]. This approach considers the total deformation of the sample as the sum of viscous, elastic and plastic deformations. Details of the deformation analysis and the adapted model have been published [11], and the total deformation during the unloading at a constant rate ($h^{UNLOAD}(t)$) is given by:

$$h^{UNLOAD}(t) = \{[(3 \times P_{max})/(4 \times R^{1/2} \times \tau_U)] \times E_r^{-2/3} \times (\Delta t)^{2/3}\} + \{b \times (\Delta t)^{5/3}\} + c \qquad (1)$$

where $\Delta t = \tau_L + \tau_U - t$, and t is the time of the measurement, τ_L and τ_U are the loading and unloading times, respectively, E_r is the reduced elastic modulus of the sample, and b and c are constants, the former depending on the geometry of the probe and the viscosity of the medium. Equation (1) was fitted to the unloading data (see examples in Figure 3) and E_r was determined. Examples of fits of this model to the experimental data are shown in Figure 3.

E_r takes into account the elastic modulus of the indenter and of the sample itself. As the indenter moduli (150 GPa for silicon [31] and 28 GPa for EBID [21]) were much greater than those of the samples (0.01-1.9 GPa), the elastic modulus of the sample (E) is approximately given by:

$$E = E_r \times (1 - v^2) \qquad (2)$$

where v is its Poisson's ratio (equal to 0.495 for Eudragit and Klucel polymer films [32]).

Elastic moduli of the films were determined based upon at least 10 indents on each of three samples. The values for Eudragit and Klucel films without MCT were 1.2 (±0.3) and 1.7

(±0.5) GPa, respectively. When 20% MCT was incorporated, the corresponding elastic moduli were 0.29-2.31 GPa and 0.31-2.37 GPa, respectively.

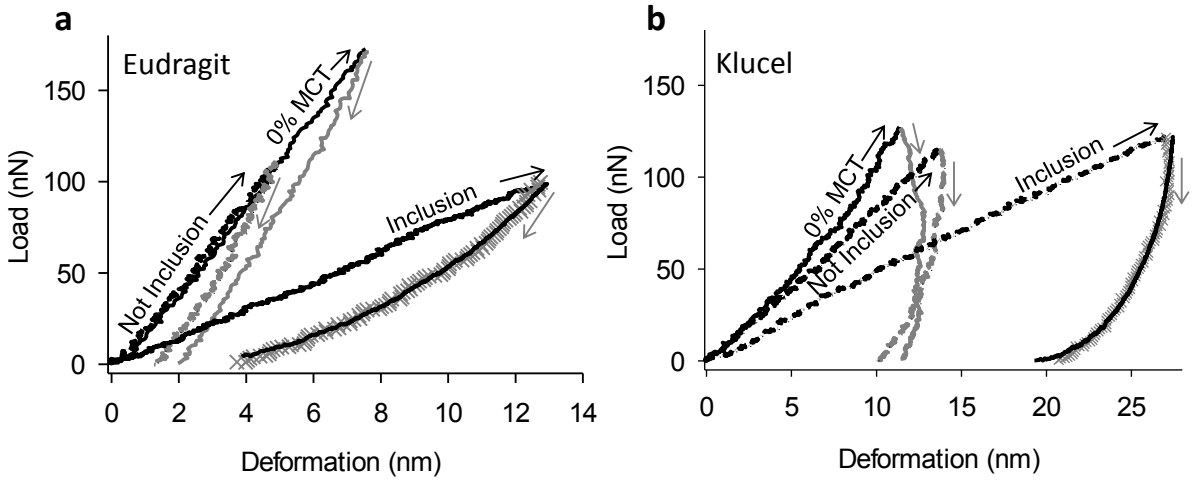

Figure 3. Load as a function of deformation during indentation of (a) Eudragit ± MCT, and (b) Klucel ± MCT. Examples of indents from areas from within and from outside the observed inclusions are shown. Data in black were collected as the load on the sample was increased (indicated by black arrows), while those in grey were recorded as the probe was retracted and the load decreased (grey arrows). The black lines intersecting grey data points for inclusion indents are model fits to the unloading data for the films with MCT.

Figure 4 shows the variation of elastic moduli across the polymer films with MCT. Indents were taken every 250 or 500 nm on a line along the film surface. As anticipated by the preceding discussion, the elastic moduli vary according to whether the indents were taken on inclusions (indicated by diagonal line shading in Figure 4) of lower elastic moduli, or on the surrounding material. The distance over which lower elastic moduli were measured agrees closely with the diameter of the inclusions observed in the AFM images.

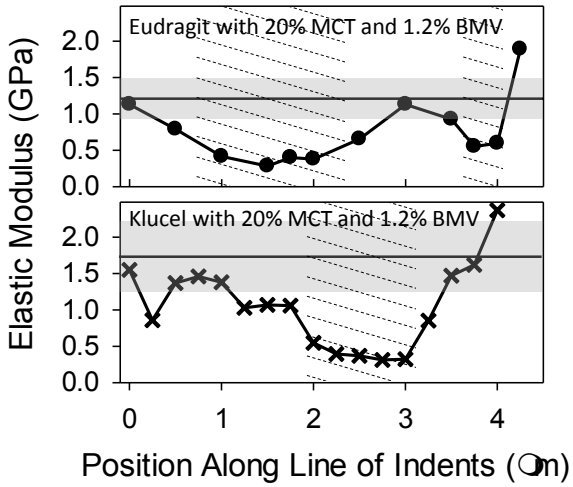

Figure 4. Elastic modulus as a function of position along a line of indents in Eudragit and Klucel films containing 20% MCT. Areas shaded with diagonal lines are considered to be inclusions. The elastic moduli of polymeric films without MCT are shown as horizontal black lines with grey shading indicating the corresponding standard deviations.

Raman micro-spectroscopy

Raman spectra

Characteristic peaks for each component of the films were identified from Raman spectra (Figures 5(a) and (c)). Spectra from inclusions and from the areas surrounding them in Eudragit and Klucel polymeric films were also recorded (Figures 5b and 5d). The presence of MCT in Eudragit films substantially increased the Raman signal between 2850 and 2890 cm^{-1} and the value at 2880 cm^{-1} was selected to monitor the distribution of this compound in the hydrophobic films. In the case of Klucel, a different peak (at 1745 cm^{-1}) was used for MCT due to overlap in the spectra at the higher wavenumber. For BMV, a peak around 1670 cm^{-1}, was used to map the distribution of drug in both polymeric films in the presence of MCT. The signal from the drug at higher wavenumbers (2800-3100 cm^{-1}) was of insufficient intensity to be of use.

Raman maps

The inclusions in the polymer films were smaller when the substrate was heated to 30°C than those observed at room temperature. As larger inclusions facilitated the Raman measurements (the resolution of the optical microscope being much lower than that of the AFM), chemical mapping was performed on films produced at room temperature.

Maps of the distributions of MCT and BMV in films are in Figure 6. Brighter pixels imply greater Raman signal intensity and hence greater concentration of the corresponding molecule. The MCT maps show that the level of this chemical was enhanced within the previously identified inclusions (Figures 6(a) and (b)). BMV was distributed throughout the films but more drug was apparent in the areas surrounding the inclusions (Figure 6(c) and (d)). The concentration of MCT varied by 50% in Eudragit films, from a normalised intensity of 1 (green pixel, the inclusions) to a normalised intensity of 0.5 (black pixel, the surroundings), and by 74% in Klucel films. The variation in BMV concentration in the films was less than for MCT: 25% and 44% in Eudragit and Klucel films, respectively. Representative variations in the intensity of the MCT and BMV signals along a line of the maps are illustrated in Figure 6(e).

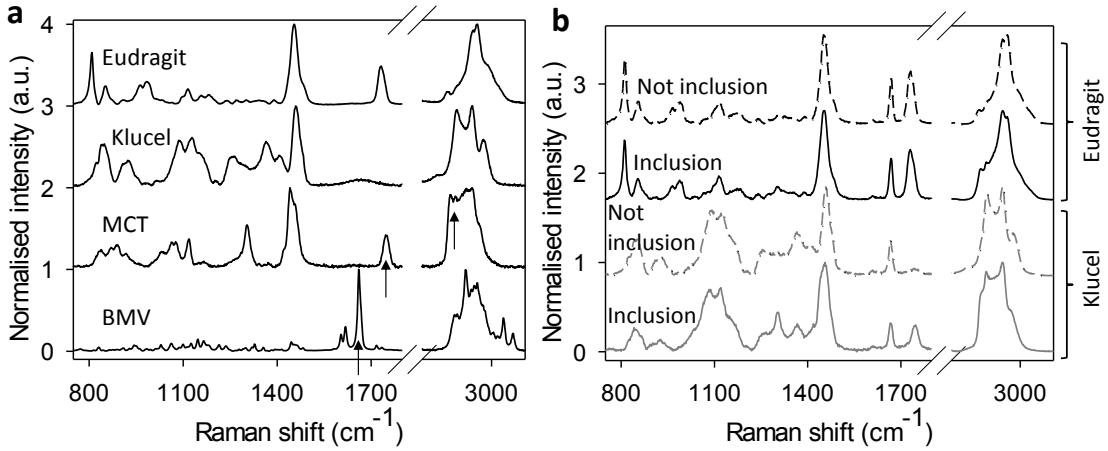

Figure 5. Raman spectra of (a) the individual constituents of the polymeric films (Eudragit, Klucel, MCT and BMV, and of (b) inclusions and the areas surrounding them in Eudragit and Klucel films incorporating MCT. Spectra have been normalised to the maximum intensity within the ranges shown, i.e., 750-1800 cm^{-1} and 2750-3120 cm^{-1}, and offset to facilitate visualisation. Arrows indicate the position of characteristic peaks for MCT and BMV.

A shift in the position of the characteristic BMV Raman peak was observed as a function of physical the state of the drug: from 1659.4 cm^{-1} and 1662.6 cm^{-1} for crystalline and amorphous solid forms, respectively, to 1665.8 cm^{-1} for the compound in solution (Figure 7(a)). Raman maps of the Eudragit and Klucel films containing MCT were produced focusing on the position of the BMV peak. In Eudragit, the drug peak position was essentially constant (1671.3 (±0.1) cm^{-1}) across the film. In contrast, in Klucel, the BMV peak varied from 1667.0 (±0.2) cm^{-1} in the inclusions to 1666.3 (±0.1) cm^{-1} in the surrounding areas (Figures 7(b) and (c)).

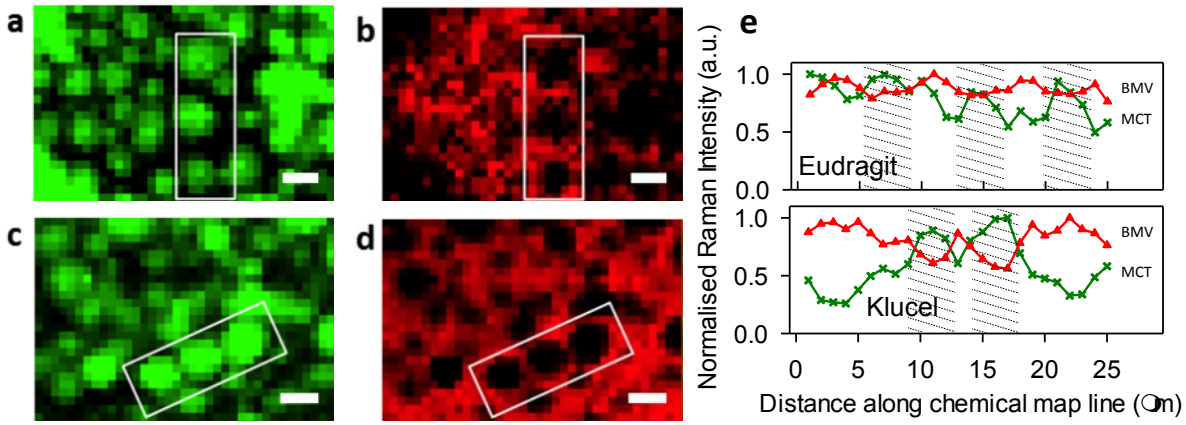

Figure 6. Raman chemical maps of the distributions of MCT and BMV in polymer films. The distributions of MCT in Eudragit and Klucel are shown in (a) and (b), respectively; the corresponding distributions of BMV are in (c) and (d). Brightly coloured green (MCT) and red (BMV) pixels indicate higher concentrations; black pixels reflect areas of lower concentrations. White boxes in the maps highlight areas with clear differentiation in chemical levels. The variations of Raman signals from MCT and BMV along the lines drawn across the maps are shown in (e), with the positions of inclusions indicated by diagonal shading. Scale bar represents 5 μm.

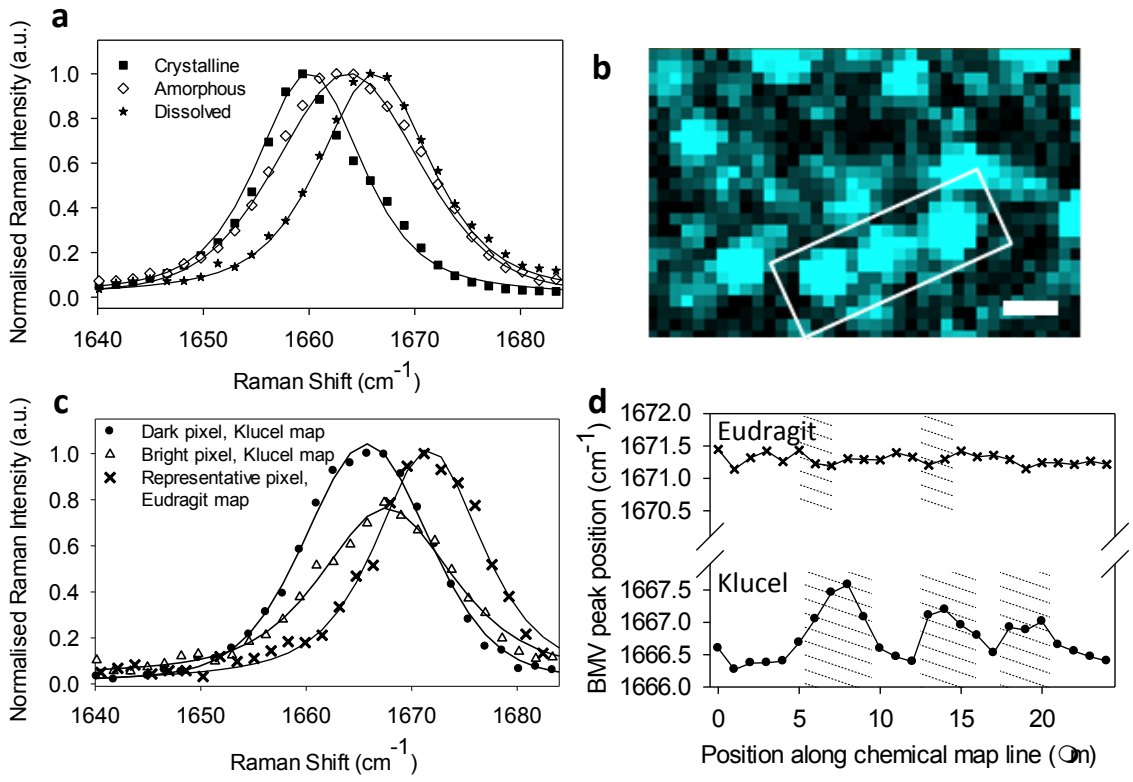

Figure 7. (a) Raman micro-spectroscopy of crystalline, amorphous and dissolved BMV. Spectra have been normalised within the range shown. (b) Raman map of the peak position of the BMV signal from a Klucel film containing MCT: the brightest pixels originate from an average peak position of 1667.6 cm^{-1}, while the dark pixels correspond to 1665.8 cm^{-1}. Scale bar represents 5 μm. (c) Representative BMV spectra from bright and dark pixels in the Raman map of a Klucel film and from a pixel in the Raman map of a Eudragit film. (d) Position of the peak characteristic of BMV in Eudragit and Klucel films along representative lines of their Raman chemical maps. Diagonally shaded areas indicate the presence of inclusions.

Skin uptake of BMV *ex vivo*

The total amount of BMV delivered into the skin (SC + epidermis + dermis) was significantly higher ($p < 0.05$) from the Eudragit FFS than either the Klucel FFS or the simple ointment (Figure 8(a)). The difference between Eudragit and the other formulations was mostly due to drug present in the SC, while the distribution into the deeper skin layers was quite similar for the three vehicles (see Supplementary Information, Figure S1). The uptake of BMV from the formulations was relatively rapid, and increased only modestly after the first 15-60 minutes of application.

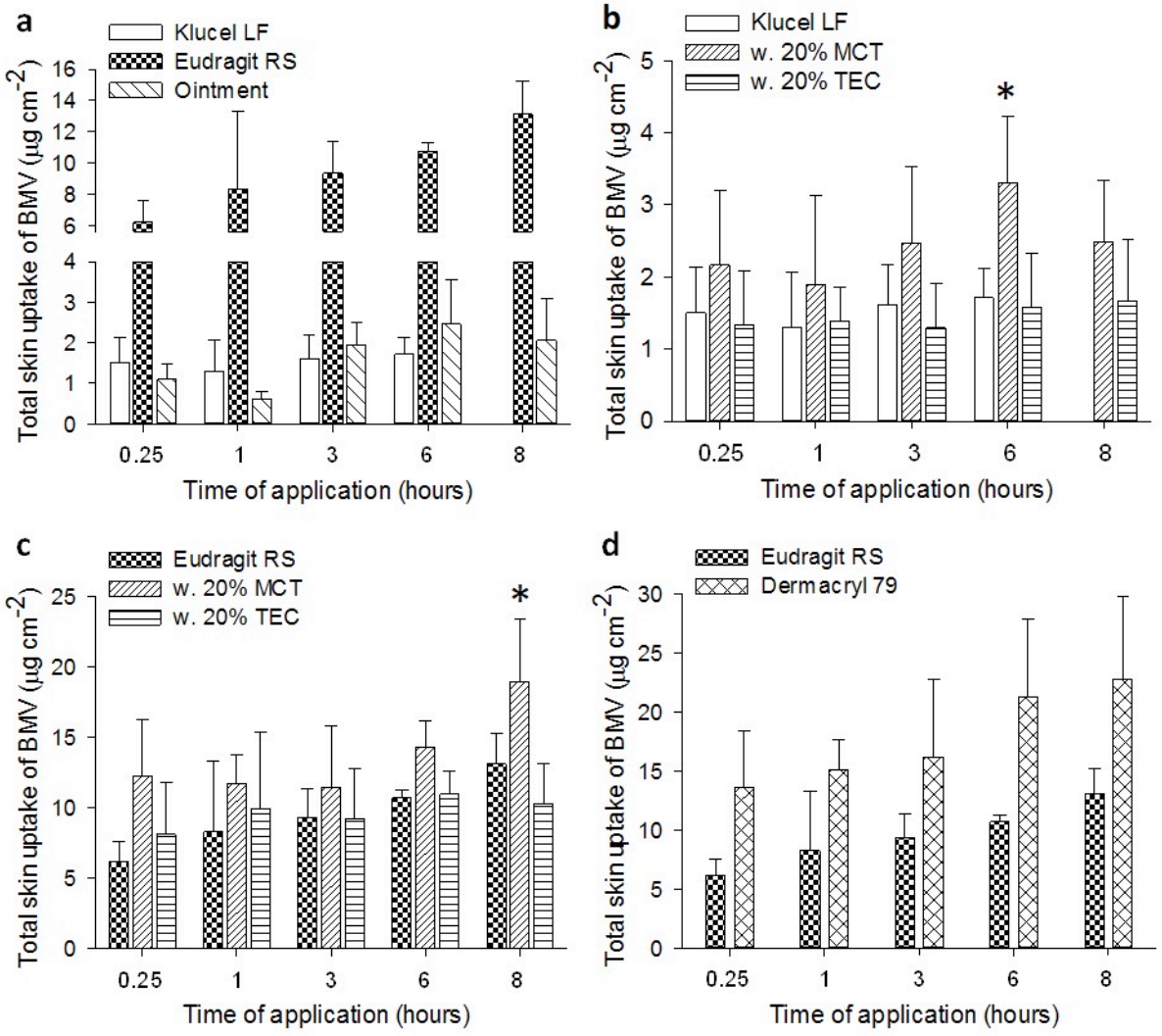

Figure 8. Skin penetration profiles of BMV after: (a) application of Klucel and Eudragit FFS and of a simple ointment; (b,c) after application of Klucel FFS (b) and Eudragit FFS (c) with and without TEC and MCT (BMV distribution into the individual skin layers (SC, epidermis, dermis) is shown in the Supplementary Information, Figures S2 and S3); (d) application of hydrophobic Eudragit and Dermacryl FFS. All values presented are the mean ± standard deviation of 4 replicates. Asterisks mark significant increases in skin uptake, relative to FFS without MCT.

Incorporation of the plasticiser (TEC) or the lipid excipient (MCT) into the Klucel and Eudragit FFS did not significantly increase BMV delivery until the period of application had reached 6 or 8 hours (Figures 8(b) and (c)) (at which point, the presence of MCT produced a significant increase in skin uptake ($p < 0.05$)).

Given that BMV delivery to the skin was greater from the more hydrophobic FFS based on Eudragit, the skin uptake of the drug was next examined from Dermacryl, an even more hydrophobic, anionic polyacrylate polymer. Like Eudragit, Dermacryl is amorphous [33], produces a FFS of low viscosity that dries to form a smooth film. *In vitro*, across an inert membrane, Dermacryl released BMV quickly at first (2.2 ± 0.4 µg cm^{-2} in 1 hour) but by 72 hours had not liberated more drug than Eudragit (4.3 ± 1.2 µg cm^{-2}). The Dermacryl FFS investigated contained 10 % w/w of polymer and did indeed deliver significantly more BMV to the skin than Eudragit as shown in Figure 8(d). It was noted, however, that the amounts

measured in the individual skin layers did not always reveal the same significant differences at all time points (see Supplementary Information, Figure S4).

BMV crystallization from polymer films

When the Klucel and Eudragit FFS were deposited on glass slides and allowed to dry, formation of BMV crystals were observed for both formulations as the films dried (see Supplementary Information, Figure S5). However, there were consistently fewer crystals seen in the Eudragit films as compared to those of Klucel. The crystal forms were also different: triangular/pyramidal habit for Klucel, irregular-shaped for Eudragit. Furthermore, when the Eudragit concentration in the FFS was increased from 5 to 15% w/w, the extent of crystallisation was decreased.

Discussion

In previous work, it was shown that the *in vitro* release of BMV was higher from a Klucel FFS than from Eudragit, and that drug release from both polymer films increased with increasing lipophilicity of the incorporated plasticiser [7]. In this work, the highly lipophilic MCT was formulated into the polymeric films, and the mechanism of enhanced drug release was elucidated. BMV release from both Klucel and Eudragit FFS incorporating MCT was significantly higher from ~6 h into the experiment (Figure 1). At 72 h, drug release from Eudragit and Klucel had been enhanced by 4.5- and 2.5-fold, respectively.

AFM and Raman micro-spectroscopy were undertaken to determine the mechanism of enhanced BMV release when MCT was incorporated into Eudragit and Klucel FFS. Earlier work [11] had shown that the plasticiser, triethyl citrate (which can reduce the glass transition temperature of polymeric films) distributed predictably and evenly throughout the polymer network. In contrast, AFM and nanoindentation experiments revealed the formation of a two-phase structure with inclusions when MCT was incorporated into Eudragit and Klucel films (Figure 2). The size of the inclusions was influenced by polymer viscosity and the temperature (and hence the rate of solvent evaporation) at which the films were prepared. For instance, larger inclusions are observed in the more viscous Klucel FFS prepared at lower temperature. In addition, the relatively poor miscibility of MCT with this more hydrophilic polymer encourages the apparent phase separation in the film and the creation of larger inclusions. The elastic moduli of those areas of the films surrounding the inclusions were similar to those of the polymers without MCT; on the other hand, the elastic moduli of the inclusions were more than three times smaller (Figure 4). Raman mapping demonstrated clearly that MCT was principally found within the inclusions; the surrounding areas comprised primarily polymer and BMV and a small proportion of MCT (Figure 5).

In Eudragit films with and without MCT, the peak of the BMV Raman signal was the same in all areas (1671.25 ± 0.11 cm^{-1}) implying that incorporation of MCT did not change the solubility of the drug in this hydrophobic polymer. Furthermore, the fractional area occupied by inclusions with respect to the total film area 0.26 (±0.15) and 0.33 (±0.03) for Eudragit and Klucel, respectively) was not significantly dependent upon the nature of the polymer. The observed enhancement in drug release rate may therefore be attributed to the presence of inclusions, their softer nature, perhaps, allowing for a higher BMV diffusivity.

For the Klucel films, the peak Raman signal from BMV (1666.26 ± 0.09 cm^{-1}) indicated that it was present in the same dissolved state in both the pure polymer and in the areas surrounding the inclusions in the polymer when MCT was present. Within the inclusions, the

shift in the peak signal (to 1667.0 ± 0.2 cm^{-1}) suggests that the ratio of dissolved to suspended drug was somewhat increased. This observation, coupled with the nanoindentation results showing the softer environment of the inclusions in Klucel (as was also seen for Eudragit), is again consistent with the enhanced release from the film in the presence of MCT. It is also noted that the difference in hardness between the inclusions and the surrounding areas of the Klucel film was smaller than that for the hydrophobic Eudragit FFS and this may explain why the relative (or fold-) improvement in drug release rate from Eudragit is more marked.

In terms of BMV delivery to the skin, Eudragit FFS delivered significantly more drug than the Klucel formulation at all times (Figure 8(a); at ≥0.25 h, $p < 0.001$). Importantly, the Eudragit FFS also significantly out-performed the conventional ointment (>0.25 h, $p < 0.05$) to a similar extent suggesting the potential to improve dermatological therapy. The amounts of BMV delivered to the skin in this study from the polymer films compare favourably with that found (1.4 μg/cm^2) after a 24-hour application of a commercial cream (Betnovate®) [34]. This observation supports the clinical relevance of the performance of the FFS examined here.

The superior outcome achieved with the more hydrophobic FFS (i.e., Eudragit) merits further analysis, particularly in light of previously published *in vitro* experiments [7], using an inert membrane, that showed a higher release of BMV from Klucel. At one level, such a divergence of behaviour confirms that there is no simple way to model the complex interactions between a formulation and the skin post-application, and that the value of *in vitro* release testing (IVRT) rests in its use as a tool for quality control, not for assessment of bioavailability and/or bioequivalence. The precise mechanism underlying the difference seen between IVRT and *ex vivo* measurements cannot be deduced unequivocally from the data obtained. Undoubtedly, the physical events occurring post-application of the FFS and the creation of the films are crucially dependent upon the formulation composition and characteristics and the nature of and the interactions with the surface onto which they are applied.

Immediately after the FFS is applied to the skin, the volatile solvent begins to evaporate, rapidly concentrating the drug, and decreasing its solubility in the vehicle to the point that saturation is reached. At this point, two scenarios are apparent: either the drug crystallises, or comes out of solution in amorphous form, or a transient, metastable, supersaturated state is formed before eventually reverting to the thermodynamically favoured situation of simple saturation. In both instances, drug uptake into the SC is driven as the solvent evaporates, and this phenomenon is manifested in the penetration profiles in Figure 8, which shows significant BMV entry into the skin within the first 15-60 minutes of application.

It is well known that certain polymers can help to stabilise, albeit transiently, a supersaturated drug solution and both Klucel [35] and Eudragit [16, 36] have been shown capable of this behaviour. Anti-nucleation efficiency of such polymers has been related to the creation of hydrogen (H)-bonds between the drug and the anti-nucleant [15, 23, 37]. The BMV crystallisation results, taken together with the higher delivery of drug, suggest that Eudragit may be able to stabilise the drug in a transient, supersaturated state better than Klucel. Inspection of the structures of the two polymers and that of the drug suggests that the H-bond donating –OH groups in BMV are matched by the H-bond accepting amine groups in Eudragit [36, 38], the equivalent of which are not found in Klucel [39]. Further support for this interpretation comes from the skin penetration data from FFS based on Dermacryl (Figure 8(d)), which performs even better than Eudragit in delivering BMV to the skin, an effect that can be attributed to the strongly H-bond accepting amide groups present in this polymer. The superior performance of the hydrophobic, acrylate-based FFS is additionally

underpinned by the generally higher solubilisation of BMV in these formulations (as compared to those with Klucel) (Figure 7(d)) and the amorphous nature of the solid drug in Eudragit.

Taken together, therefore, the above factors result in a superior drug delivery performance by Eudragit and Dermacryl, with a transient period of BMV supersaturation achieved that permits establishment of a drug reservoir in the SC from which a sustained, but slower, release over an extended period of time may be achieved; equally, the more favourable solubility characteristics of BMV in the residual formulations of these hydrophobic polymers on the skin surface ensures that the drug can continue to be made available after the 'metamorphosis' [2] of the FFS has been completed.

With respect to incorporation of a plasticiser, or a lipid excipient, into the FFS, while TEC has been shown to increase the release of BMV from polymeric films in vitro [7], the plasticiser did not increase the skin penetration of the drug ($p > 0.05$). Nonetheless, TEC does impart flexibility to the film [11], an important feature with respect to the comfort of the drug delivery system on the skin. IVRT of polymeric FFS indicated that drug liberation increased with increasing lipophilicity of the incorporated plasticiser [7]. MCT was also rather effective when included in the FFS tested and this ability was confirmed in the *ex vivo* experiments described here: significant improvement ($p < 0.05$) in BMV delivery into the skin was observed (Figures 8(c) and 8(d)) for both Klucel and Eudragit FFS at the longest applications studied (6 and 8 h, respectively).

Finally, further consideration of the AFM nanoindentation studies of Klucel and Eudragit polymeric films incorporating MCT and the biphasic structure with the lipid excipient concentrated into inclusions. While these measurements were made on films cast on a glass slide, it is plausible to anticipate that the observed phase separation, at least to some extent, also occurs when the polymeric films are formed on skin. This would mean that BMV solubilised in the mechanically softer inclusions might be more easily and rapidly released (relative to the more rigid polymeric surroundings). Raman micro-spectroscopic mapping of Klucel and Eudragit films incorporating MCT showed that the relative distribution of MCT in Klucel was approximately 4:1 in favour of the inclusions (relative to the 'stiffer' surroundings), but was only about 2:1 for Eudragit. The corresponding values for BMV were roughly 2:1 (in Klucel) and ~1.3:1 (in Eudragit) in favour of the areas surrounding the inclusions. As a result, the drug-to-excipient ratios in Klucel and Eudragit were 0.46 and 0.64, respectively (a schematic illustrating these calculations is provided in the Supplementary Information, Figure S6). The implications of these findings are (at least) two-fold. First of all, as one might expect, the miscibility of the lipid excipient in Eudragit is superior to that with the more hydrophilic Klucel. Second, even though the higher MCT level in the Klucel inclusions makes these regions softer than the corresponding areas in the Eudragit films, more BMV is found in the latter and this means that drug delivery from the hydrophobic FFS is the most efficient. Overall, therefore, one can conclude that the judicious incorporation of a lipophilic excipient into a FFS formulation can enhance the delivery of relatively lipophilic drugs into the skin.

Conclusions

The drug release enhancing effect of MCT *in vitro* when incorporated in Eudragit and Klucel FFS has been demonstrated, and AFM and Raman micro-spectroscopy have provided complementary information on the mechanism by which this is achieved. The films adopt a two-phase structure when MCT is present, comprising softer inclusions within a surrounding, more solid polymeric network. MCT is primarily located within the soft inclusions. BMV distributes throughout the films, but at relatively higher levels in the polymeric network surrounding the inclusions. Enhanced drug release from the films in the presence of MCT was attributed to the formation of the inclusions, their softer environment presumably leading to a higher diffusivity of the drug. BMV appears to be more soluble (relative to the surrounding areas) in the inclusions in Klucel films from which drug release was highest.

The topical delivery of a common, lipophilic corticosteroid (BMV) into the skin from these polymeric films (FFS) formed *in situ* was subsequently demonstrated. The superior performance of FFS formed with hydrophobic polymers, specifically Eudragit and Dermacryl, is apparent (relative to a FFS prepared with the more hydrophilic Klucel). The results suggest that the rapid skin uptake of the drug is facilitated by a transient period of supersaturation favoured by hydrogen bond interactions between BMV and the hydrophobic acrylate polymers employed. It is suggested that this mechanism allows for the establishment of drug 'reservoirs' both in the residual polymeric film on the skin surface, and within the stratum corneum, from which sustained delivery can then be maintained over an extended period. Incorporation of a lipophilic excipient (medium-chain triglyceride) into the hydrophobic polymer films enhances BMV uptake into the skin at the longer periods of application considered. In summary, the research described provides a foundation upon which further formulation development and optimisation can be based and more detailed studies may be planned *in vivo*.

Acknowledgements

This work was financially supported by LEO Pharma A/S (Ballerup, Denmark) and the University of Bath, Faculty of Science Graduate School (Bath, England). We thank Lene Midjord Olsen for invaluable assistance with the penetration studies. Klucel™ LF and Eudragit® RS polymers were provided gratis by the manufacturers.

References

[1] R.C. Wester, H.I. Maibach, Cutaneous Pharmacokinetics - 10 Steps to Percutaneous-Absorption, Drug Metabolism Reviews, 14 (1983) 169-205.

[2] C.D. Surber, A. F., Bioavailability and bioequivalence of dermatological formulations, in: K.A. Walters (Ed.) Dermatological and transdermal formulations, Marcel Dekker, New York, 2002, pp. 401-498.

[3] I.Z. Schroeder, P. Franke, U.F. Schaefer, C.M. Lehr, Delivery of ethinylestradiol from film forming polymeric solutions across human epidermis in vitro and in vivo in pigs, J. Controlled Release, 118 (2007) 196-203.

[4] A. Misra, R.S. Raghuvanshi, S. Ganga, M. Diwan, G.P. Talwar, O. Singh, Formulation of a transdermal system for biphasic delivery of testosterone, J. Controlled Release, 39 (1996) 1-7.

[5] C. Padula, G. Colombo, S. Nicoli, P.L. Catellani, G. Massimo, P. Santi, Bioadhesive film for the transdermal delivery of lidocaine: in vitro and in vivo behavior, J. Controlled Release, 88 (2003) 277-285.

[6] D. Lunter, R. Daniels, In vitro Skin Permeation and Penetration of Nonivamide from Novel Film-Forming Emulsions, Skin Pharmacology and Physiology, 26 (2013) 139-146.

[7] K. Frederiksen, R.H. Guy, K. Petersson, Formulation considerations in the design of topical, polymeric film-forming systems for sustained drug delivery to the skin, Eur. J. Pharm. Biopharm., 91 (2015) 9-15.

[8] J.K. Sears, J.R. Darby, The technology of plasticizers, Wiley, New York, 1982.

[9] T. Mahnaj, S.U. Ahmed, F.M. Plakogiannis, Evaluating the efficacy of a group of nontraditional plasticizers on the glass transition temperature of ethyl cellulose polymer, Drug Dev. Ind. Pharm., 37 (2011) 342-350.

[10] H.O. Ammar, M. Ghorab, S.A. El-Nahhas, R. Kamel, Polymeric Matrix System for Prolonged Delivery of Tramadol Hydrochloride, Part I: Physicochemical Evaluation, Aaps Pharmscitech, 10 (2009) 7-20.

[11] H. Garvie-Cook, K. Frederiksen, K. Petersson, R.H. Guy, S. Gordeev, Characterization of topical film-forming systems using atomic force microscopy and Raman microspectroscopy, Mol. Pharm., 12 (2015) 751-757.

[12] S. Wiedersberg, A. Naik, C.S. Leopold, R.H. Guy, Pharmacodynamics and dermatopharmacokinetics of betamethasone 17-valerate: assessment of topical bioavailability, British Journal of Dermatology, 160 (2009) 676-686.

[13] V.M. Masterson, X.P. Cao, Evaluating particle hardness of pharmaceutical solids using AFM nanoindentation, Int. J. Pharm., 362 (2008) 163-171.

[14] B. Bhushan, W. Tang, S. Ge, Nanomechanical characterization of skin and skin cream, Journal of Microscopy, 240 (2010) 135-144.

[15] J.H. Kim, H.K. Choi, Effect of additives on the crystallization and the permeation of ketoprofen from adhesive matrix, Int. J. Pharm., 236 (2002) 81-85.

[16] M.A. Pellett, S. Castellano, J. Hadgraft, A.F. Davis, The penetration of supersaturated solutions of piroxicam across silicone membranes and human skin in vitro, J. Controlled Release, 46 (1997) 205-214.

[17] F. Cilurzo, P. Minghetti, A. Casiraghi, L. Tosi, S. Pagani, L. Montanari, Polymethacrylates as crystallization inhibitors in monolayer transdermal patches containing ibuprofen, Eur. J. Pharm. Biopharm., 60 (2005) 61-66.

[18] K. Moser, K. Kriwet, Y.N. Kalia, R.H. Guy, Stabilization of supersaturated solutions of a lipophilic drug for dermal delivery, Int. J. Pharm., 224 (2001) 169-176.

[19] A.F. Davis, J. Hadgraft, Effect of Supersaturation on Membrane-Transport .1. Hydrocortisone Acetate, Int. J. Pharm., 76 (1991) 1-8.

[20] J.E. Sader, J.W.M. Chon, P. Mulvaney, Calibration of rectangular atomic force microscope cantilevers, Rev. Sci. Instrum., 70 (1999) 3967-3969.

[21] J.D. Beard, S.N. Gordeev, Large flexibility of high aspect ratio carbon nanostructures fabricated by electron-beam-induced deposition, Nanotechnology, 21 (2010).

[22] M.L. Oyen, R.F. Cook, Load-displacement behavior during sharp indentation of viscous-elastic-plastic materials, J. Mater. Res., 18 (2003) 139-150.

[23] L.A. Wegiel, L.J. Mauer, K.J. Edgar, L.S. Taylor, Crystallization of amorphous solid dispersions of resveratrol during preparation and storage-Impact of different polymers, J. Pharm. Sci., 102 (2013) 171-184.

[24] P. Minghetti, F. Cilurzo, S. Pagani, A. Casiraghi, R. Assandri, L. Montanari, Formulation study of oxybutynin patches, Pharm. Dev. Technol., 12 (2007) 239-246.

[25] U. Jacobi, M. Kaiser, R. Toll, S. Mangelsdorf, H. Audring, N. Otberg, W. Sterry, J. Lademann, Porcine ear skin: an in vitro model for human skin, Skin Research and Technology, 13 (2007) 19-24.

[26] C. Herkenne, A. Naik, Y.N. Kalia, J. Hadgraft, R.H. Guy, Pig ear skin ex vivo as a model for in vivo dermatopharmacokinetic studies in man, Pharm. Res., 23 (2006) 1850-1856.

[27] V. Klang, J.C. Schwarz, B. Lenobel, M. Nadj, J. Aubock, M. Wolzt, C. Valenta, In vitro vs. in vivo tape stripping: Validation of the porcine ear model and penetration assessment of novel sucrose stearate emulsions, Eur. J. Pharm. Biopharm., 80 (2012) 604-614.

[28] L.B. Jensen, K. Petersson, H.M. Nielsen, In vitro penetration properties of solid lipid nanoparticles in intact and barrier-impaired skin, Eur. J. Pharm. Biopharm., 79 (2011) 68-75.

[29] S. Wiedersberg, C.S. Leopold, R.H. Guy, Dermatopharmacokinetics of betamethasone 17-valerate: Influence of formulation viscosity and skin surface cleaning procedure, Eur. J. Pharm. Biopharm., 71 (2009) 362-366.

[30] W.C. Oliver, G.M. Pharr, Measurement of hardness and elastic modulus by instrumented indentation: Advances in understanding and refinements to methodology, J. Mater. Res., 19 (2004) 3-20.

[31] A.L. Weisenhorn, S. Kasas, J.M. Solletti, M. Khorsandi, V. Gotzos, D.U. Romer, G.P. Lorenzi, Deformation observed on soft surface with an AFM, 1993.

[32] M. Geerligs, L. van Breemen, G. Peters, P. Ackermans, F. Baaijens, C. Oomens, In vitro indentation to determine the mechanical properties of epidermis, Journal of Biomechanics, 44 (2011) 1176-1181.

[33] L.L. Sperling, Introduction to physical polymer science, 4th ed., John Wiley & Sons, New Jersey, 2005.

[34] M.L. Reid, F. Benaouda, R. Khengar, S.A. Jones, M.B. Brown, Topical corticosteroid delivery into human skin using hydrofluoroalkane metered dose aerosol sprays, Int. J. Pharm., 452 (2013) 157-165.

[35] N.A. Megrab, A.C. Williams, B.W. Barry, Estradiol Permeation through Human Skin and Silastic Membrane - Effects of Propylene-Glycol and Supersaturation, J. Controlled Release, 36 (1995) 277-294.

[36] P.N. Kotiyan, P.R. Vavia, Eudragits: Role as crystallization inhibitors in drug-in-adhesive transdermal systems of estradiol, Eur. J. Pharm. Biopharm., 52 (2001) 173-180.

[37] A. Misra, R. Pal, S.S. Majumdar, G.P. Talwar, O. Singh, Biphasic testosterone delivery profile observed with two different transdermal formulations, Pharm. Res., 14 (1997) 1264-1268.

[38] U.S. Kestur, L.S. Taylor, Role of polymer chemistry in influencing crystal growth rates from amorphous felodipine, CrystEngComm, 12 (2010) 2390-2397.

[39] B. Van Eerdenbrugh, L.S. Taylor, An ab initio polymer selection methodology to prevent crystallization in amorphous solid dispersions by application of crystal engineering principles, CrystEngComm, 13 (2011) 6171-6178.

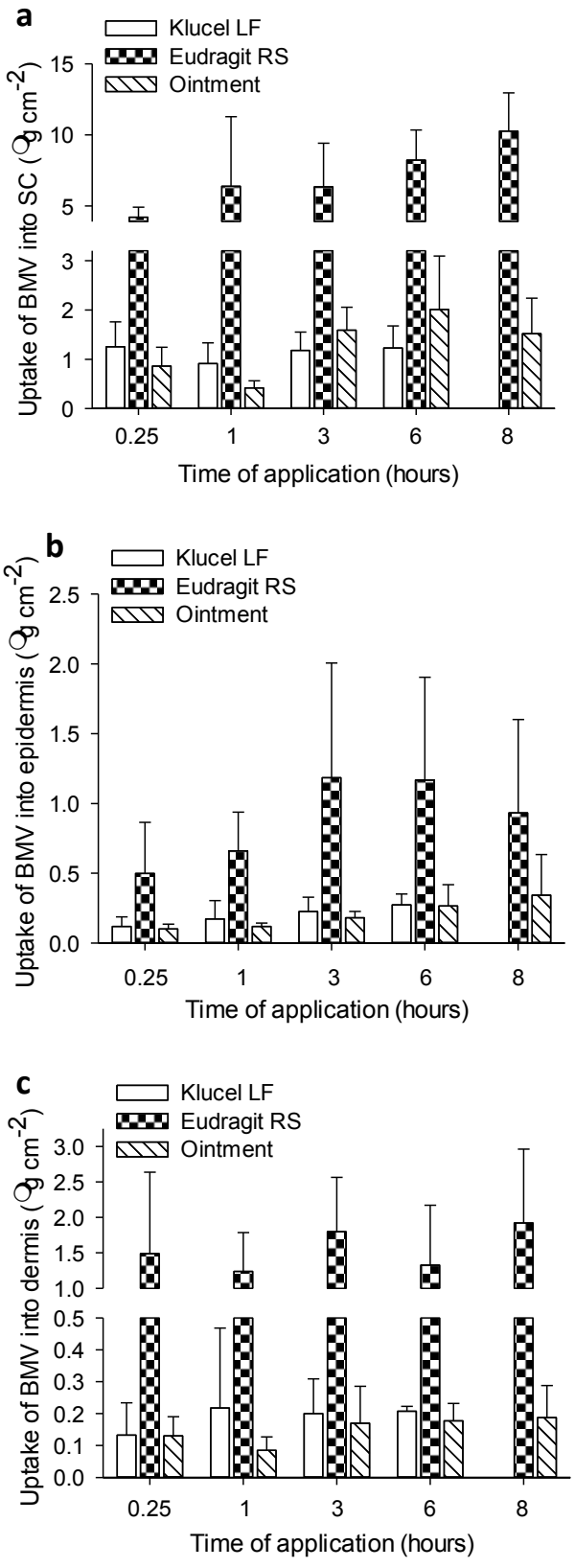

Supplementary Figure S1. Penetration profiles of BMV into the (a) SC, (b) epidermis and (c) dermis after topical application of FFS and ointment (mean ± standard deviation; n=4).

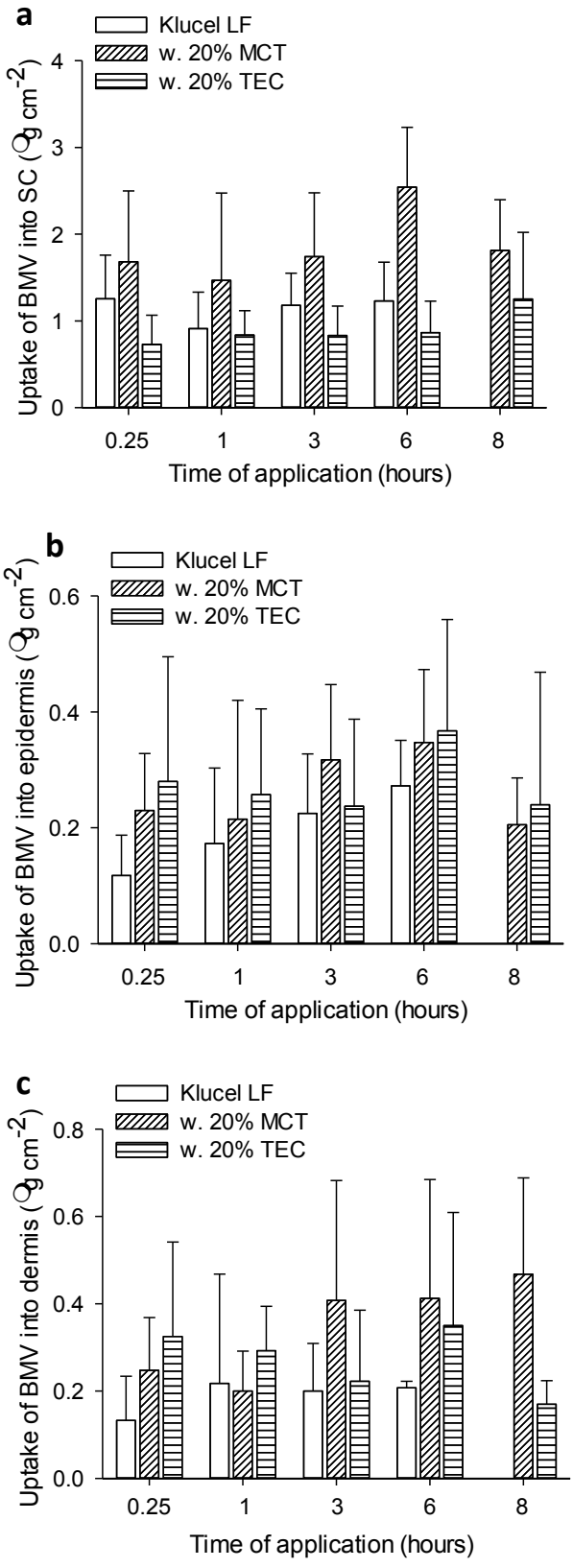

Supplementary Figure S2. Penetration profiles of BMV into the (a) SC, (b) epidermis and (c) dermis after topical application of Klucel FFS with and without TEC and MCT, plasticizer and lipid, respectively (mean ± standard deviation; n=4).

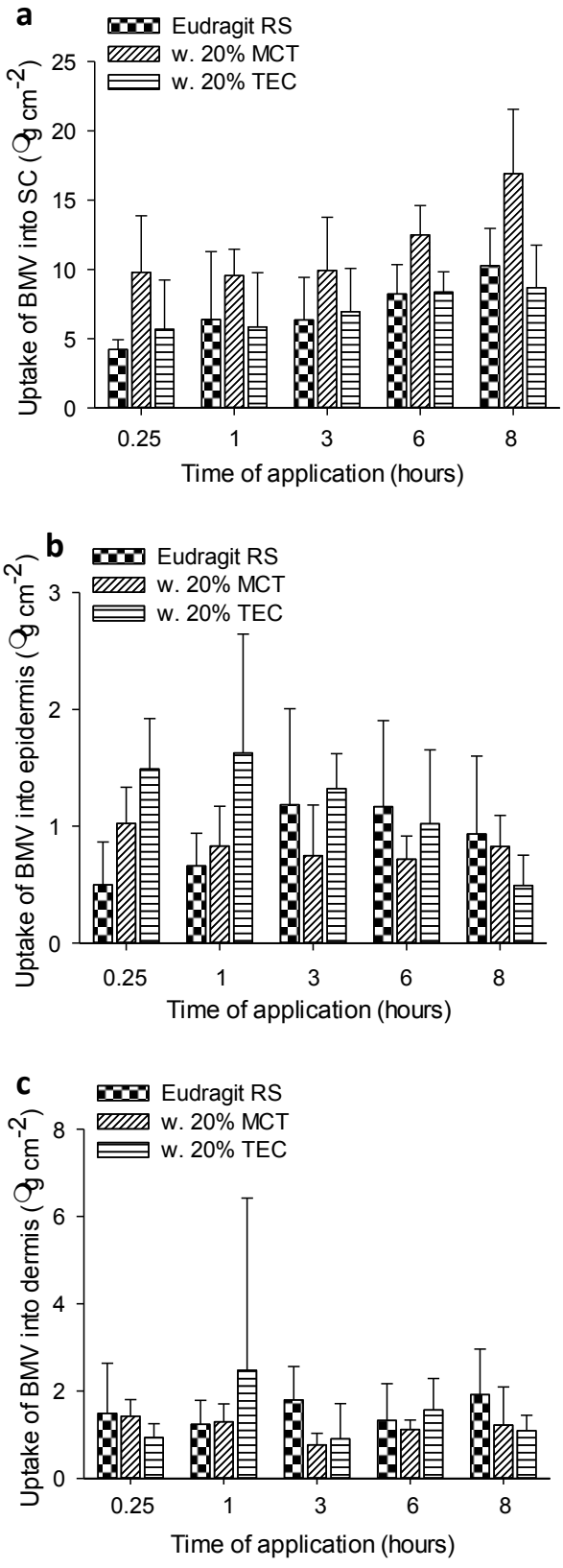

Supplementary Figure S3. Penetration profiles of BMV into the (a) SC, (b) epidermis and (c) dermis after topical application of Eudragit FFS with and without TEC and MCT, plasticizer and lipid, respectively (mean ± standard deviation; n=4).

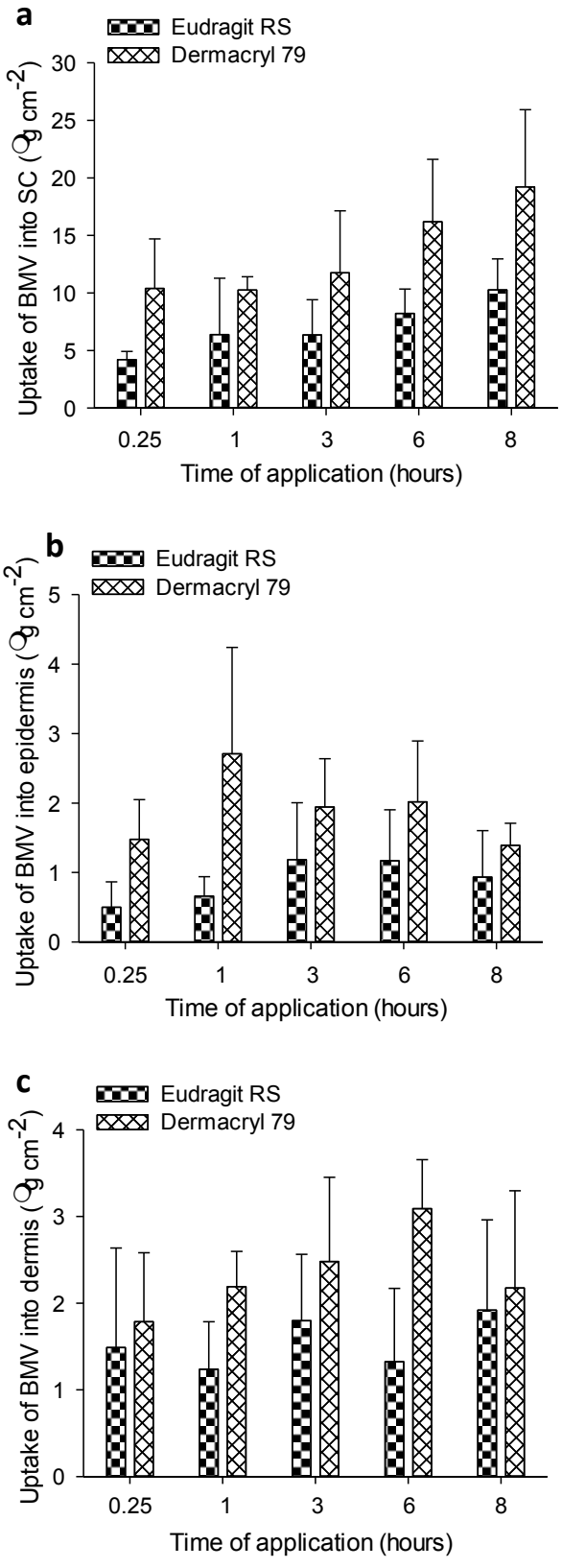

Supplementary Figure S4. Penetration profiles of BMV into the (a) SC, (b) epidermis and (c) dermis after topical application of hydrophobic FFS, Eudragit and Dermacryl (mean ± standard deviation; n=4).

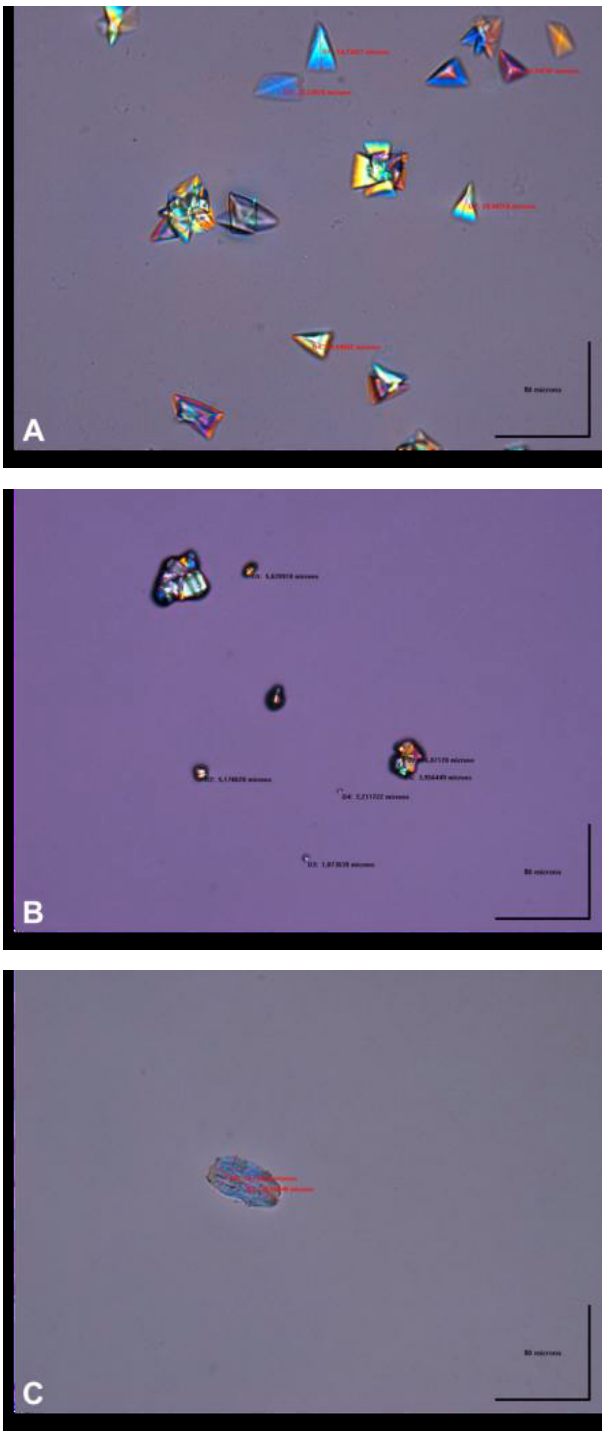

Supplementary Figure S5. Representative micrographs showing BMV crystallisation from polymeric FFS: (a) 5% w/w Klucel, (b) 5% w/w Eudragit and (c) 15% w/w Eudragit. The concentration of the drug in ethanol, 5% w/w Klucel FFS, 5% w/w Eudragit FFS and 15% w/w Eudragit FFS was 6.07% w/w (corresponding to 5% w/w betamethasone). Scale bar represents 50 μm.

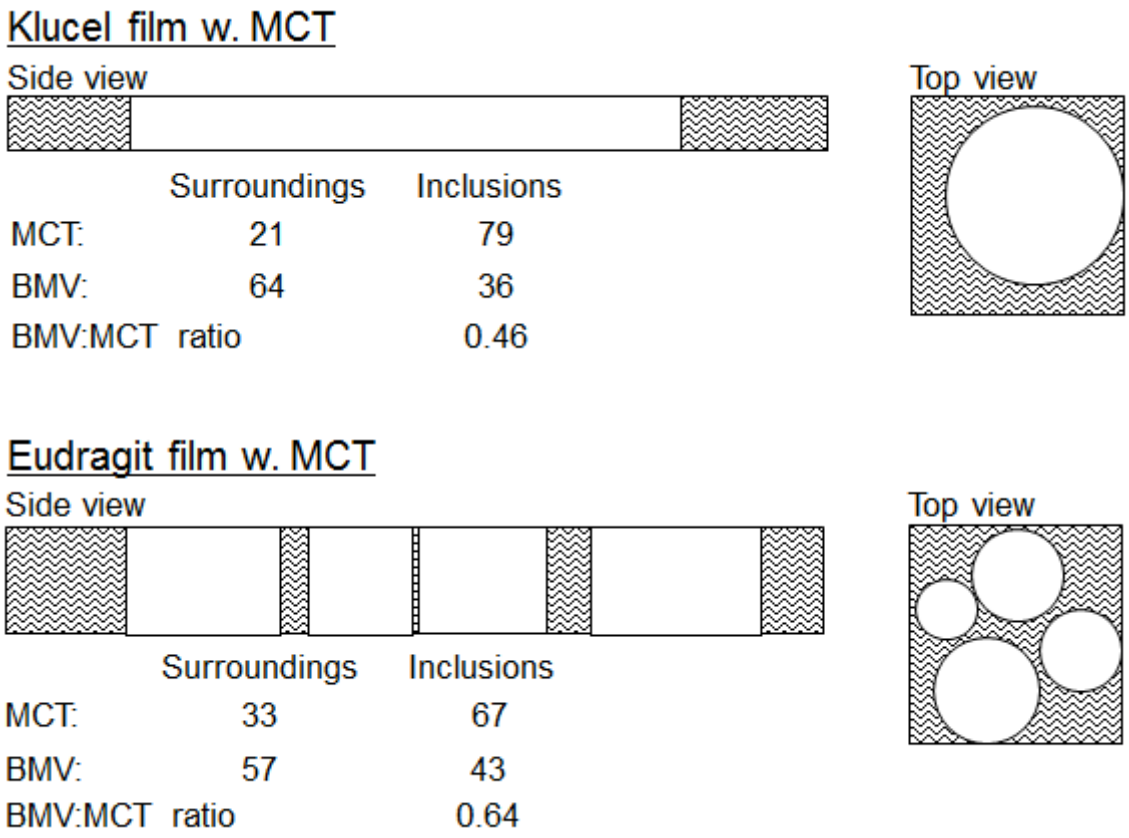

Supplementary Figure S6. Schematic representation (not to scale) of biphasic Klucel (upper panel) and Eudragit (lower panel) films. The shaded and white areas represent the 'rigid' surroundings and the softer inclusions, respectively. The relative distributions of MCT and BMV in the inclusions and the surroundings have been deduced from Raman chemical mapping. Note that this illustration of the inclusions assumes that they are cylindrical in form; this may not necessarily be the case (e.g., they may be spherical or ovoid) and this would alter (quantitatively but not qualitatively) the calculated relative distributions of MCT and BMV.